Published in final edited form as:
Nat Immunol. 2019 November ; 20(11): 1435–1443. doi:10.1038/s41590-019-0493-z.

House dust mites activate nociceptor-mast cell clusters to drive type 2 skin inflammation

Nadine Serhan[1,#], **Lilian Basso**[1,#], **Riccardo Sibilano**[2,3], **Camille Petitfils**[4], **James Meixiong**[5], **Chrystelle Bonnart**[4], **Laurent L. Reber**[6,7], **Thomas Marichal**[8,9], **Philipp Starkl**[10,11], **Nicolas Cenac**[4], **Xinzhong Dong**[5,12], **Mindy Tsai**[2,3], **Stephen J. Galli**[2,3,13,#], **Nicolas Gaudenzio**[1,#]

[1]Unité de Différenciation Epithéliale et Autoimmunité Rhumatoïde (UDEAR), UMR 1056, INSERM, Université de Toulouse, Toulouse, France

[2]Department of Pathology, Stanford University School of Medicine, Stanford, CA 94305, USA

[3]Sean N. Parker Center for Allergy and Asthma Research, Stanford University School of Medicine, CA 94305, USA

[4]IRSD, Université de Toulouse, INSERM, INRA, INP-ENVT, Université de Toulouse 3 Paul Sabatier, Toulouse, France

[5]The Solomon H. Snyder Department of Neuroscience, Center for Sensory Biology Johns Hopkins University, School of Medicine, Baltimore, MD 21205, USA

[6]Department of Immunology, Unit of Antibodies in Therapy and Pathology, Institut Pasteur, Paris, France; INSERM, U1222, Paris, France

[7]Center for Pathophysiology Toulouse Purpan, INSERM U1043, CNRS UMR 5282, Toulouse III University, Toulouse, France

[8]GIGA Institute and Faculty of Veterinary Medicine, Liege University, Liege, Belgium

[9]WELBIO, Walloon Excellence in Life Sciences and Biotechnology, Wallonia, Belgium

[10]CeMM Research Center for Molecular Medicine of the Austrian Academy of Sciences

Correspondence should be addressed to: Nicolas Gaudenzio, Immception Lab (www.immception.com), UDEAR, UMR 1056 Inserm - Université de Toulouse, Hôpital Purpan, Place du Dr Baylac - TSA 40031, 31059 Toulouse cedex 9 – France, Tel: +33 (0)561158426, nicolas.gaudenzio@inserm.fr or Stephen J. Galli, 269 Campus Drive, CCSR Room 3255b, Stanford, CA 94305-5176, USA, Telephone: (650) 736-6014, sgalli@stanford.edu.
[#]The following authors contributed equally

Life Sciences Reporting Summary. Further information on experimental design and reagents is available in the Life Sciences Reporting Summary.

Data availability. The data that support the findings of this study are available from the corresponding author Nicolas Gaudenzio upon request.

Competing interests
The authors declare no competing interests.

Author contributions
SJG and NG conceived the project. All authors were involved in experimental design. NS, LB and NG performed most experiments and compiled the data. RS, CB, JM, CP, TM, PS, LLR, NC, XD and MT helped with experiments. All authors participated in analyzing the data and writing or editing the paper.

Europe PMC Funders Author Manuscripts

[11]Laboratory of Infection Biology, Department of Medicine I, Medical University of Vienna, 1090, Vienna, Austria

[12]Howard Hughes Medical Institute, Johns Hopkins University School of Medicine, Baltimore, MD 21205, USA

[13]Department of Microbiology & Immunology Stanford University School of Medicine, Stanford, CA 94305, USA

Abstract

Allergic skin diseases, such as atopic dermatitis (AD), are clinically characterized by severe itching and type 2 immunity-associated hypersensitivity to widely-distributed allergens, including those derived from house dust mites (HDMs). Here we found that HDMs with cysteine-protease activity directly activated peptidergic nociceptors, which are neuropeptide-producing nociceptive sensory neurons, that expressed the ion channel TRPV1 and *Tac1*, the gene encoding the precursor for the neuropeptide substance P. Intravital imaging and genetic approaches indicated that HDMs-activated nociceptors drove the development of allergic skin inflammation by inducing the degranulation of mast cells contiguous to such nociceptors through the release of substance P and the activation of the cationic molecules receptor MRGPRB2 on mast cells. This data indicates that, after exposure to HDM allergens, activation of TRPV1^{+}*Tac1*$^{+}$ nociceptor-MRGPRB2^{+} sensory clusters represents a key early event in the development of allergic skin reaction.

Altered tissue sensitivity to environmental triggers is thought to contribute to the development of allergic inflammation, frequently starting with type 2 (allergic) skin diseases such as atopic dermatitis (AD)[1] during childhood. AD is a chronic relapsing skin inflammatory disease characterized by severe itching of the skin, eczema and hypersensitivity to otherwise innocuous environmental substances[2]. The etiology of AD is incompletely understood, but many factors, such as genetic or environmental elements and immune or structural cells are thought to contribute to the development of skin lesions[2].

Aberrantly activated type 2 immunity against common sources of indoor allergens such as house dust mites (HDMs) and increased numbers of activated mast cells and eosinophils in the lesional skin[2–4] might have important roles in the pathology of AD. Moreover, 80-100% of patients with AD are colonized with *Staphylococcus aureus,* compared to only 5-30% of healthy individuals[5], and patients whose skin is colonized with exotoxin-producing *S. aureus*, such as staphylococcal enterotoxins B (SEB)[4,6,7] have a higher severity of AD than patients who are colonized with non-toxigenic strains[6]. Finally, although abnormalities of the epidermis leading to loss of skin barrier have been reported to contribute to skin lesions development[8,9,10], many patients with AD don't have loss-of-function mutations of epidermal structural proteins such as filaggrin[11–13]. Therefore, the full spectrum of factors which contribute to skin barrier disorganization and the development of type 2 immunity and skin lesions remains to be determined.

The skin is innervated by an intricate network of nociceptive sensory neurons, known as nociceptors, with cell bodies located in the dorsal root or trigeminal ganglia[14]. Their primary function is the transmission of sensations of temperature, pain and itch in order to elicit

appropriate behavioral responses such as withdrawal (to avoid tissue injury) and scratching (to remove irritants). Nociceptors may be involved in manifestations of AD by promoting itch and scratching behavior[13,15], an idea supported by clinical studies showing that the serum of patients with AD exhibits high amounts of neuropeptides, such as the cationic neuropeptide substance P (SP), and that the amounts detected correlate with the severity of the disease[15,16]. While much remains to be learned about itching sensations, peripheral neurons also have the potential to influence immune cells and inflammatory responses[17–22].

Mast cells are innate immune cells thought to be involved in allergic diseases, including AD, in which they recognize a specific antigen through their high-affinity receptors for IgE (FcεRI)[23]. Under homeostatic conditions, skin and peritoneal mast cells in mice specifically express MRGPRB2, a receptor for cationic molecules from the Mas-related G protein-coupled receptors family[24]. MRGPRX2, the human ortholog of MRGPRB2, and not the neurokinin 1 receptor, is the main receptor for cationic molecules, including SP, in human skin mast cells[25,26]. MRGPRX2 or MRGPRB2-mediated activation of mast cells can result in a remarkably fast degranulation dynamics, which is associated with the development of rapid and localized mast cell-dependent inflammation[25].

Whether specialized neuro-immune cross-talk has a role in the development of allergic skin inflammation remains unclear. Combining genetically-modified mouse models with intravital imaging approaches, we show here that a large proportion of $TRPV1^+$ nociceptor projections form physical contacts with $MRGPRB2^+$ mast cells. These neuro-immune clusters can sense the presence of allergic cues and can trigger pathogenic type 2 immune responses and associated lesions in the skin.

Results

Tac1 expression is required for allergic skin inflammation

We used a mouse model of allergic skin inflammation driven by six epicutaneous exposures over one month to two antigens found together in the lesional skin of 80-100% of AD patients[2–7,26], 10 μg of the HDM strain *Dermatophagoides farinae* (*D. farinae*) and 500 ng of the bacterial exotoxin SEB from *S. aureus* (Supplementary Fig. 1a,b). Compared to healthy subjects, AD patients often suffer from *S. aureus* skin infections which are thought to play an important role in the pathogenesis and/or worsening of AD[6]. This model recapitulates moderate to severe AD-like disease, associated with both the histopathological features of an exacerbated type 2 immune response and a global gene expression pattern statistically similar to that seen in human AD[8,27]. Wild-type mice sensitized with a combination of SEB and *D. farinae* developed more severe skin inflammation than those treated with SEB or *D. farinae* alone, while *D. farinae* alone induced more skin lesions than SEB alone (Supplementary Fig. 1c,d). Compared to vehicle, treatment with *D. farinae* + SEB induced a systemic *D. farinae*-specific T_H2 response (Supplementary Fig. 1e,f). In accord with reports that patients with moderate to severe AD were treated successfully with dupilumab[28], a human monoclonal antibody against the IL-4 receptor α (IL-4Rα) that inhibits both IL-4 and IL-13 signaling, systemic treatment with blocking antibodies for the mouse IL-4Rα significantly decreased the skin lesions and the histopathological features in the AD-like mouse model (Supplementary Fig. 1g,h). These data indicate that treatment with *D. farinae*

+ SEB leads to the development of AD-like allergic skin inflammation dependent on type 2 cytokines.

The neuropeptide SP is thought to be released primarily from a unique subpopulation of $TRPV1^+$ $TRPA1^-$ peptidergic nociceptors that highly express *Tac1*[29], the gene encoding the SP precursor. Using publicly available gene expression data[30], we mapped the expression of *Trpv1*, *Tac1* and *Trpa1* among different mouse tissues and various subpopulations of immune cells. *Trpv1*, *Tac1* and *Trpa1* were highly (or exclusively, in the case of *Trpv1* and *Trpa1*) expressed in dorsal root ganglia (DRG), where the somas of sensory neurons are located, with weak additional expression of *Tac1* in the central and the enteric nervous systems (Fig. 1a and Supplementary Fig. 1i). In whole-mounted skin biopsies from C57BL/6J wild-type mice, SP expression was restricted to $PGP9.5^+$cutaneous neuronal fibers (Fig. 1b).

To analyze the role of SP in the development of allergic skin inflammation, we treated wild-type and $Tac1^{-/-}$ mice with *D. farinae* + SEB and assessed the development of key pathological features associated with AD[8]. Compared to vehicle-treated wild-type mice, *D. farinae* + SEB-treated wild-type mice developed macroscopic skin lesions (Fig. 1d), increased epidermal thickness, strong infiltration of eosinophils and neutrophils (Fig. 1e) and elevated serum *D. farinae*-specific IgG_1 and IgE (Fig. 1f), along with a profound alteration of filaggrin protein expression (Fig. 1g,h), a key component of skin barrier function linked to human AD[12]. In addition, *D. farinae* + SEB-treated wild-type mice had increased expression of keratin 6 (K6), a marker of inflammatory stress in keratinocytes (Supplementary Fig. 2a,b) and alterations in claudin-1, K14 and K10 expression (Supplementary Fig. 2c-h). Expressions of two other structural proteins loricrin and E-cadherin were not significantly affected (Supplementary Fig. 2i-l). By contrast, *D. farinae* + SEB-treated $Tac1^{-/-}$ mice were mostly protected from disease, with substantial reduction in skin lesion development, histological abnormalities, infiltration of immune cells, serum levels of *D. farinae*-specific IgG_1 and IgE and changes in skin barrier architecture (Fig. 1c-h and Supplementary Fig. 2). Taken together, this data suggested that expression *of Tac1* and SP was restricted to the neuronal compartment of the skin and that expression of *Tac1* was required for the full development of the pathological features associated with allergic skin inflammation in this model.

HDMs directly activate substance P-producing $TRPV1^+$ neurons

To analyze the role of $TRPV1^+$ nociceptors in the development of allergic skin inflammation, we treated wild-type mice systemically with resiniferatoxin (RTX), which is a potent TRPV1 agonist selectively ablating $TRPV1^+$ nociceptors[17,18] (Supplementary Fig. 3a,b). RTX-treated mice and control DMSO-treated mice were subsequently treated with *D. farinae* + SEB to induce allergic skin inflammation. RTX-treated mice had a strong reduction of skin lesions (Fig. 2a,b) and lesion-associated histopathological features compared to control DMSO-treated mice (Fig. 2c), along with restored filaggrin organization and decreased expression of the stress marker K6 (Supplementary Fig. 3), suggesting that $TRPV1^+$ nociceptors were required for the full development of allergic skin inflammation in this model.

The primary function of nociceptors is to detect potentially damaging stimuli and initiate appropriate behavioral responses such as removal or scratching. We investigated whether *D. farinae* and SEB were directly detected by TRPV1$^+$ DRG neurons cultured *ex vivo*. We found that 5 ng/ml SEB alone induced only a weak (barely detectable in some experiments) influx of calcium in DRG neurons (Fig. 2d,e), while concentrations ranging from 5 ng/ml of *D. farinae*, either alone (Fig. 2d,f) or in combination with 5 ng/ml SEB (Fig. 2d,g) triggered an increase in intracellular calcium in a subpopulation of DRG neurons that also responded to the TRPV1 agonist capsaicin (Fig. 2h,i).

D. farinae alone or in combination with SEB also triggered the secretion of SP from DRG neurons, with a tendency, in some experiments, for *D. farinae* + SEB to trigger less secretion of SP compared to either alone (Fig. 2j). Moreover, cultured DRG neurons from RTX-treated mice did not secrete SP in response to *D. farinae* alone or *D. farinae* + SEB, while DRG neurons from DMSO-treated mice secreted SP (Fig. 2k). Importantly, DRG neurons from RTX-treated mice were also unresponsive to capsaicin (Fig. 2k) indicating that *in vivo* RTX-treatment efficiently depleted TRPV1$^+$ neurons. These data indicated that *D. farinae* directly triggered the secretion of SP from TRPV1$^+$ DRG neurons cultured *ex vivo*.

Next, we investigated by which mechanism *D. farinae* activated TRPV1$^+$ DRG neurons. Treatment of DRG neurons with NBP2-29328, a MYD88 inhibitory peptide[8], did not prevent *D. farinae*-induced activation of DRG neurons compared to DRG neurons treated with a non-relevant control peptide (Supplementary Fig. 4a,b), indicating that, at least under the culture conditions used here, DRG neurons activation was not dependent on MYD88-dependent signaling through Toll like receptors (TLR). Next, we investigated whether the proteolytic activity of *D. farinae* was required for triggering DRG neuron activation *ex vivo*. Like other common environmental allergens, HDM strains, including *D. farinae*[31] have intrinsic proteolytic activity that can degrade epithelial junctions[32–35] or full-length IL-33[36] *in vivo*. To characterize the type of proteolytic activity present in the *D. farinae* extracts used, we measured the proteolytic activities of *D. farinae* with or without specific and irreversible inhibitors of cysteine or serine protease activities. Pretreatment with the cysteine protease inhibitor E64, but not with the serine protease inhibitor AEBSF, completely inhibited the proteolytic activity of *D. farinae*, at levels comparable to heat-inactivation of *D. farinae* (Fig. 3a). No proteolytic activity was measured in the absence of dithiothreitol (DTT), a reducing agent required for cysteine protease activity in cell-free conditions (Fig. 3a), indicating the presence of cysteine protease activities in the *D. farinae* extract. SEB alone neither exhibited protease-like activity nor enhanced *D. farinae* proteolytic activity (Supplementary Fig. 4c).

Heat-induced inactivation or treatment with E64 prevented the influx of calcium in TRPV1$^+$ DRG neurons by *D. farinae ex vivo* (Fig. 3b-e). However, TRPV1$^+$ DRG neurons activation was independent of the expression of the protease-activated receptor PAR2 by the neurons (Supplementary Fig. 4a,b). We next investigated whether other clinically-relevant environmental allergens with either predominant cysteine protease activity, such as the HDM strain *D. pteronyssinus*[31] or serine-like protease activities[36] from pollen (ragweed), fungus (*Alternaria alternata*) or the German cockroach could also directly activate DRG neurons. Only *D. pteronyssinus* triggered significant influx of calcium in DRG neurons, comparable

to those obtained after stimulation with *D. farinae* (Fig. 3f). These data indicate that two common HDM strains with predominant cysteine protease activity involved in allergic inflammation and suspected to have major roles in various allergic disorders, could trigger the activation of a subset of nociceptors directly, predominantly via a cysteine protease activity-dependent mechanism.

Functional MRGPRB2 is required for allergic skin inflammation

Mouse MRGPRB2 and its human ortholog, MRGPRX2 are mast cell-restricted receptors for several cationic substances, including the neuropeptide SP. We used *Kit*-dependent $Kit^{W\text{-}sh/W\text{-}sh}$ mast cell-deficient mice, in which KIT, the receptor for the main mast cell growth and survival factor SCF is mutated, and *Kit*-independent *Cpa3*-Cre^{+}*Mcl-1*$^{fl/fl}$ mast cell-deficient mice, in which the antiapoptotic factor Mcl-1 is deleted in the mast cell lineage (Supplementary Fig. 5 and Supplementary Fig 6a-d) to study the role of mast cells in the development of allergic skin inflammation. After treatment with *D. farinae* + SEB, both $Kit^{W\text{-}sh/W\text{-}sh}$ and *Cpa3*-Cre^{+}*Mcl-1*$^{fl/fl}$ mice had a marked reduction in skin lesions compared to $Kit^{+/+}$ and *Cpa3*-Cre^{-}*Mcl-1*$^{fl/fl}$ littermate controls, respectively (Supplementary Fig. 5). Importantly, *Tac1*$^{-/-}$ mice or RTX-treated wild-type mice had normal numbers of dermal mast cells (Supplementary Fig. 6e,f), indicating that the reduced pathological features in these mice after treatment with *D. farinae* + SEB could not be attributed simply to a lack or reduction in the number of skin mast cells.

To assess whether MRGPRB2 contributed to the development of allergic skin inflammation, we used *Mrgprb2*$^{mut/mut}$ mice, in which MRGPRB2 is genetically inactivated by mutation, but have normal numbers of mast cells[24] (Supplementary Fig. 6g,h). In contrast to *Mrgprb2*$^{+/+}$littermates, *Mrgprb2*$^{mut/mut}$ mice did not develop allergic skin inflammation after treatment with *D. farinae* + SEB, and had substantial reductions in skin lesions (Fig. 4a,b), histological abnormalities, infiltration of eosinophils and neutrophils (Fig. 4c), *D. farinae*-specific IgE (Fig. 4d) and disruption of skin barrier architecture (Fig. 4e,f and Supplementary Fig. 7), suggesting that MRGPRB2 expressed on mast cells contributed to the development of this model of allergic skin inflammation induced by *D. farinae* + SEB.

TRPV1^{+} nociceptors activate skin mast cells through MRGPRB2

We next explored whether *D. farinae* and SEB triggered the degranulation of dermal mast cells *in vivo* through the activation of TRPV1^{+}*Tac1*$^{+}$ nociceptors and MRGPRB2. A single intradermal (i.d.) injection of sulforhodamine 101-labeled avidin (Av-SRho) can be used to monitor skin mast cell granule structures specifically in live mice by two-photon microscopy or *ex vivo* by confocal microscopy[37]. We injected vehicle or 1 μg *D. farinae* + 50 ng SEB i.d. into the ear pinna of Av.SRho-injected mice and measured tissue swelling, as an early readout of inflammation and Av.SRho^{+} mast cell degranulation in whole-mounted ear skin using *ex vivo* volumetric confocal microscopy 45 minutes post *D. farinae* + SEB injection (Supplementary Fig. 8a). I.d. injection of vehicle induced very mild swelling of the ear tissue (Fig. 5a) and did not trigger substantial skin mast cell degranulation (Fig. 5b,c) in DMSO-treated wild-type mice or *Mrgprb2*$^{+/+}$ mice, while injection of *D. farinae* + SEB induced strong ear swelling (Fig. 5a) and abundant degranulation of Av.SRho^{+} mast cells (Fig. 5b,d). After injection of *D. farinae* + SEB, RTX-treated wild-type mice or

Mrgprb2$^{mut/mut}$ mice had a substantial reduction of both ear swelling (Fig. 5a) and degranulation of Av.SRho^{+} mast cells (Fig. 5b,d) compared to DMSO-treated wild-type or *Mrgprb2*$^{+/+}$ mice. Wild-type mice injected i.d. with blocking antibodies against SP had a strong reduction of both ear swelling (Fig. 5e) and mast cell degranulation (Fig. 5f,g) compared to IgG isotype-treated control mice. In addition, a 30 minute pretreatment of *D. farinae* + SEB with the cysteine protease inhibitor E64 decreased ear swelling significantly (Supplementary Fig. 8b,c). *D. farinae* and/or SEB did not trigger the degranulation of *in vitro*-cultured mouse or human mast cells at the tested concentrations (Supplementary Fig. 8d,e).

We next tested whether activation of TRPV1^{+} nociceptors in the skin using the TRPV1 agonist capsaicin would result in MRGPRB2-dependent mast cell degranulation *in vivo*. I.d. injection of 1 μM capsaicin did not induce significant ear tissue swelling (Fig. 5h) or Av.SRho^{+} mast cell degranulation (Fig. 5i,j) in RTX-treated wild-type mice or *Mrgprb2*$^{mut/mut}$ mice, while strong ear swelling (Fig. 5h) and linked degranulation of Av.SRho^{+} mast cells (Fig. 5i,j) were observed in DMSO-treated wild-type and *Mrgprb2*$^{+/+}$mice, indicating that the effect was largely dependent on TRPV1^{+} nociceptors and MRGPRB2. These results indicate that, upon i.d. injection of *D. farinae* + SEB or capsaicin, the observed mast cell degranulation and associated early signs of inflammation require functional TRPV1^{+} nociceptors, release of SP and signaling through MRGPRB2.

Next, we adapted the fluorescent avidin-based mast cell imaging approach to visualize the activation of TRPV1^{+} nociceptors and the activation of mast cells simultaneously using intravital two-photon microscopy[37]. For this purpose we used Pirt-GCaMP3 mice, in which expression of the calcium tracer GCaMP3 is driven by the *Pirt* promoter in sensory neurons[38] in order to track the spatiotemporal dynamics of skin mast cell granule structures and TRPV1^{+} nociceptors activation in living mice (Supplementary Fig. 8f). Low basal expression of GCaMP3 fluorescence (Fig. 6a,b and Supplementary Fig. 8g) in sensory neurons, but no degranulation of Av.SRho^{+} mast cells (Fig. 6a,c and Supplementary Fig. 8h) were detected after i.d. injection of vehicle. In contrast, i.d. injection of 1 μM of the TRPV1 agonist capsaicin induced strong increases in GCaMP3 fluorescence (Fig. 6a,b and Supplementary Fig. 8g), revealing the presence of an abundant network of activated TRPV1^{+} nociceptors in the mouse dermis, as well as degranulation of ~50-60 % of Av.SRho^{+} mast cells (Fig. 6a,c and Supplementary Fig. 8h). After i.d. infusion of 1 μg *D. farinae* + 50 ng SEB, either in combination or separately, in Av.SRho-labelled Pirt-GCaMP3 mice we observed a significant increase in GCaMP3 fluorescence in skin neurons compared to vehicle-injected mice (Fig. 6a,b) and degranulation of ~ 50% Av.SRho^{+} mast cells (Fig. 6a,c), suggesting that the presence of *D. farinae* and/or SEB antigens in the dermis could lead to the activation of TRPV1^{+} nociceptors and mast cells *in vivo*. Finally, we used an automated computer-assisted calculation method to perform an unbiased analysis of the spatial organization of activated TRPV1^{+} nociceptors and Av.SRho^{+} mast cells in the dermis of Pirt-GCaMP3 mice as assessed by live imaging. About 62 % of Av.SRho^{+} mast cells either formed contacts with activated TRPV1^{+} nociceptors in the skin (25%) or resided in close proximity to activated nociceptors (37% of Av.SRho^{+} mast cells were within less than 25 μm from activated TRPV1^{+} nociceptors) (Fig. 6d-f). These data suggest that mast cells and TRPV1^{+} nociceptors formed cellular clusters in the skin that can be activated in the

presence of *D. farinae* and SEB. Together, these results indicated that the ear swelling observed upon i.d. injection of *D. farinae* + SEB resulted from the activation of skin TRPV1$^+$ nociceptors which induced the degranulation of mast cells through the release of SP and the activation of MRGPRB2.

Discussion

Here we found that TRPV1$^+$ *Tac1*$^+$ nociceptors and MRGPRB2$^+$ mast cells formed clusters in the mouse skin that could be activated by allergens, such as HDMs. This, in turn, drove the development of type 2 immunity-associated skin inflammation in mice that mimicked many features of human AD. In addition, our results identified MRGPRB2 as a key receptor that facilitated communication between skin mast cells and TRPV1$^+$ *Tac1*$^+$ nociceptors.

Based on the generated high-resolution 3D images, it is interesting to speculate that the close anatomical co-localization of mast cells and TRPV1$^+$ nociceptors in the mouse dermis might enable the accumulation of high enough amounts of secreted neuropeptide such as SP to reach the previously reported high activation threshold of MRGPRB2[39]. Fixed biopsies have indicated proximity or contact between nerve fibers and mast cells in mice, pigs and humans[40–43], while mouse and human mast cells can be directly activated by neuropeptides (including SP) *in vitro*[25,42,44]. A bi-directional activation process between mast cells and submucosal neurons in cultured gut biopsies has been reported[45]. Our study offers direct evidence of functional interactions between nociceptors and mast cells *in vivo* and identified these interactions as a critical element in the development of type 2 skin inflammation. Targeting SP-enabled interactions between TRPV1$^+$ nociceptors and MRGPRX2$^+$ mast cells might therefore represent a promising therapeutic approach for the prevention and/or treatment of human AD pathology.

Recent studies have reported that MRGPRB2 on mast cells has an important role in the regulation of inflammatory pain[46] and itch sensation[47]. SP and MRGPRB2 were reported to be directly involved in the regulation of inflammatory mechanical and thermal hyperalgesia, and in the recruitment of innate immune cells at the site of injury[46]. In addition, compared to activation through canonical FcεRI, mast cell activation through MRGPRB2 induces itch distinct from classical histaminergic itch[47]. MRGPRB2-mediated activation of mast cells results in the differential release of granule-associated mediators (including some with known pruritogen function such as histamine, serotonin or tryptase), and MRGPRB2 deficiency significantly decreases itch in different models of allergic contact dermatitis, which is thought to be associated with pathogenic CD8$^+$ T cell responses[48]. These observations indicate that MRGPRB2 activation on mast cells modulates the transmission of sensations of pain and itch in different inflammatory contexts.

Mast cells can drive certain types of IgE-independent pseudo-allergic reactions through the binding of a wide range of cationic drugs (such as the FDA-approved mivacurium or icatibant) to MRGPRX2 or MRGPRB2[24,49,50]. It is tempting to speculate that MRGPRX2 or MRGPRB2-mediated mast cell activation by cationic drugs could lead to the activation of nociceptors at the site of injection and the subsequent development of pain and/or itch. However, more *in vivo* work is needed to define whether the clusters of TRPV1$^+$ *Tac1*$^+$

nociceptors and MRGPRB2^{+} mast cells described here are involved in drug-induced adverse events.

We found that *D. farinae*, but not SEB, directly activated TRPV1^{+} DRG neurons *ex vivo* through a cysteine protease-dependent mechanism. We can't rule out the possibility that direct effects of *D. farinae* and/or SEB on skin mast cells, apart from effects on degranulation, also may have contributed to our findings. However, the data presented suggest that, under the conditions studied, *D. farinae* + SEB-induced cutaneous inflammation required TRPV1^{+} nociceptors and the release of SP, which then activated skin mast cells.

Most patients with severe AD are colonized with exotoxin-producing *S. aureus*[4,6,7]. In agreement to that, we found that *D. farinae* in combination with SEB triggered the development of more severe skin inflammation than when the two antigens were used separately. While SEB alone did not activate DRG neurons cultured *ex vivo*, after i.d. injection *in vivo* it triggered GCaMP3 fluorescence in skin neurons comparable to that observed after injection of *D. farinae*. This might indicate that SEB activated nociceptors through an indirect mechanism; however, the precise mechanism(s) remain(s) to be elucidated. It is possible that SEB, which is known to be a potent superantigen, could also favor the proliferation of T cells in our model. However, SEB treatment alone in wild-type mice triggered less severe skin inflammation and skin lesions than treatment with *D. farinae* alone. It is therefore possible that a direct mechanism of nociceptor activation by *D. farinae* cysteine protease activity might be required to efficiently trigger the development of this model of *D. farinae* + SEB-induced allergic skin inflammation.

The sensing of allergen-associated proteolytic activity has been proposed to be an important mechanism of environmental allergen detection that could contribute to the initiation of allergic diseases[31,36]. Our data suggest that the clusters of TRPV1^{+} nociceptors and MRGPRB2^{+} mast cells might represent tissue-resident "sensory systems" that would detect allergens with cysteine-like protease activity in the skin and initiate type 2 immunity-associated allergic skin disease. Sensory nerve fibers and mast cells are also present in the upper airways, lungs and gastro-intestinal tract, which are organs continuously exposed to environmental allergens and within which allergic diseases are also known to develop. However, the extent to which neuron-mast cell clusters are involved in the development of other allergic disorders in different organs remains to be investigated.

Methods

Mice

Four- to 8-week-old C57BL/6J and *Tac1*$^{-/-}$ mice were purchased from Charles River or the Jackson Laboratory; both age-matched male and female mice were used in experiments. *Mrgprb2*$^{mut/mut}$ mice (which are homozygous for a mutation that induces a genetic inactivation of *Mrgprb2*[24]) and Pirt-GCaMP3 mice (in which a genetically encoded calcium tracer [GCaMP3] is driven into sensory neurons by the *Pirt* promoter[38]) were provided by X. Dong and both male and female mice were used in experiments. The mast cell-deficient *Kit*$^{W\text{-}sh/W\text{-}sh}$ and *Cpa3-cre*$^{+}$*;Mcl-1*$^{fl/fl}$ mice have been described previously[25,37]; both male

and female mice were used in experiments. PAR-2-deficient mice were a generous gift from N. Vergnolle. Mice were bred and housed in the local animal facilities of CREFRE (Toulouse, France) or Stanford University (CA, USA), and littermate control mice were used in all experiments. All animal care and experimentation were conducted in France and in the USA. Experiments conducted in USA (Galli Lab, Stanford University, CA) were in compliance with the guidelines of the National Institutes of Health (NIH) and the Institutional Animal Care and Use Committee of Stanford University. Experiments conducted in France (Gaudenzio Lab, INSERM, University of Toulouse) were in compliance with the guidelines of the European Union (86/609/EEC) and the French Committee of Ethics (87/848) policies and with the specific approval from the local ministry-approved committee on ethics in animal experimentation (Ethics Committee UMS006 CEEA-122, project n° 13283 2018031416055447V3). 8 to 12-week-old mice were used in experiments, excepted for RTX treatment for which 4-week-old mice were used.

Reagents and antibodies

Sodium citrate, Bovine Serum Albumin (BSA), DMSO, saponin, Capsaicin, Resiniferatoxin and Staphylococcal Enterotoxin B (SEB) were from Sigma-Aldrich. HDM extracts of the strain *Dermatophagoides farinae* were purchased from Greer Laboratories. The following antibodies were obtained from Covance: anti-Keratin (K) 14, anti-K6, anti-K10, anti-loricrin and anti-filaggrin. Anti-Claudin 1 was from Abcam. Alexa594-conjugated goat anti-rabbit IgG, Alexa488-conjugated avidin and DAPI were from Life Technologies Invitrogen. The following reagent and antibodies were from eBioscience Thermofisher Scientific: CellTrace™ CFSE Cell Proliferation Kit, anti-CD4-APC, anti-IL4-PE, anti-IL-5-PE, anti-IL-13-PE, and anti-IFNγ-PE. Purified NA/LE Rat Anti-Mouse CD124 (mIL4R-M1) or control Istoype (R35-95) were from BD Bioscience. MYD88 inhibitory peptide (i.e., a cell permeant peptide sequence that selectively blocks MYD88 homodimerization) and a control peptide (i.e., an inactive and cell permeant truncated form of the MYD88 inhibitory peptide) were from Novus. *Alternaria alternata (A. alternata), Dermatophagoides pteronyssinus (D. pteronyssinus)*, ragweed and German Coackroach were all from Stallergenes Greer.

Model of allergic skin inflammation

Allergic skin inflammation was induced as previously described[8,27] (described in Supplementary Fig. 1). Briefly, back skin was shaved and a solution of 500 ng of Staphylococcal enterotoxin B (SEB, Sigma-Aldrich) and of 10 μg of *Dermatophagoides farinae* extract (HDM, Stallergen Greer) in PBS was applied on a gauze pad placed on the shaved back and occluded with a Tegaderm™ Transparent Dressing (3M HealthCare). Three days later, the gauze pads were replaced. Mice were monitored on a daily basis and if a mouse removed the bandage, a new dressing was immediately applied on this mouse and all of the other mice within the same experiment (so that they received the same treatment and equal amounts of antigens). Four days later, dressings were removed and mice were kept without treatment for the next week. This "3 + 4 days" pattern of treatment was repeated two more times, so that the mice were subjected to three cycles of such treatment. Two days after the last cycle of treatment, the mice were euthanized and back skin specimens corresponding to the treated areas were obtained for analyses. In a set of experiments, mice were also treated with either IgG isotype control or anti-CD124 antibody (100 μL; i.p.) at 2.8 mg/kg

twice a week for the entire period of treatment. The last treatment with either of these antibodies was done one day before sacrifice. This model has been efficiently used in both Inserm Toulouse and Stanford University and key experiments have been repeated in both animal facilities.

Ablation of Trpv1$^+$ nociceptors in mice

To ablate Trpv1$^+$ nociceptors, 4-week-old C57BL/6J mice were subcutaneously injected with increasing resiniferatoxin (RTX) doses of 30 μg/kg, 70 μg/kg and 100 μg/kg in 100 μL of PBS for 3 consecutive days. Control mice were injected with similar volumes of DMSO in 100 μL of PBS. 4 weeks later, denervation was assessed using the classical tail flick assay.

Peripheral blood mononuclear cell-derived human mast cell culture

Peripheral blood mononuclear cells were obtained from buffy coats of healthy blood donors at the Etablissement Francais du Sang (EFS) and were cultured as described in *Gaudenzio et al.*[25]. Briefly, isolated CD34$^+$ cells (EasySep Human CD34 Positive Selection Kit, STEMCELL Technologies) were cultured for one to two weeks in StemSpan medium (STEMCELL Technologies) supplemented with recombinant human IL-6 (50 ng/ml; Peprotech), human IL-3 (10 ng/ml; Peprotech), ciprofloxacin (10 μg/ml; Sigma-Aldrich) and 3% supernatant of CHO transfectants secreting mouse SCF. After two weeks, cells were transferred to IMDM Glutamax supplemented with sodium pyruvate, 2-β-mercaptoethanol (50 μM), 0.5% BSA, 1% insulin transferrin selenium (all from Invitrogen), ciprofloxacin (10 μg/ml; Sigma-Aldrich), IL-6 (50 ng/ml) and 3% supernatant of Chinese hamster ovary (CHO) transfectants secreting mouse SCF. Mast cells were usually ready for experiments after ~10 weeks in culture.

Bone marrow-derived cultured mouse mast cells (BMCMCs)

Hematopoietic cells were collected from C57BL/6 mouse femurs and cultured in DMEM supplemented with L-Glutamax, 2-β-mercaptoethanol (50 μM; Invitrogen), murine IL-3 (10 ng/mL; Peprotech), 10% Fetal Bovine Serum (FBS, Invitrogen) and Peni/Strep (100X). Twenty-four hours later, adherent cells were removed, and fresh culture medium was added to non-adherent cells. Three days later, cells were resuspended in fresh culture medium. The same procedure was repeated twice a week. Cells were used for experiments between week 4 and week 10.

β-Hexosaminidase release assay

Human mast cells were incubated in culture medium with or without human IgE (1 μg/mL; Sigma-Aldrich) overnight at 37°C. BMCMCs were incubated with or without anti-dinitrophenol (DNP) IgE (0.5 μg/mL; Sigma Aldrich) overnight at 37°C. The cells were then washed and distributed in 96-well flat-bottom plates at a density of 10^5 cells in 50 μL of Tyrode's buffer at 37°C. 40 minutes later, cells were treated with 50 μL of prewarmed stimuli diluted in Tyrode's buffer for 45 minutes at 37°C. As a positive control of functional activation, human mast cells were stimulated with anti-IgE (10 ng/mL; Euromedex) and BMCMCs with DNP-BSA (10 ng/mL; Sigma Aldrich). To assess whether AD antigens could activate mast cells, human mast cells and BMCMCs were stimulated with increasing

concentrations of *D. farinae* and SEB (5 ng/mL, 50 ng/mL and 500 ng/mL), alone or together. β-Hexosaminidase release in the supernatants was measured as previously described[25].

Intracellular flow cytometry of *D. farinae*-specific CD4$^+$ T cells

Following induction of allergic skin inflammation, spleens from vehicle-treated or *D. farinae* + SEB-treated mice were harvested and dissociated to obtain a suspension of cells. 200,000 spleen cells were stained with CFSE for 7 minutes at 37°C and incubated for 5 days with 10 μg/ml of *D. farinae* in RPMI 1640 supplemented with 10% FCS GlutaMAX-I, sodium pyruvate, 2-mercaptoethanol, and 10μg/ml ciprofloxacin. Intracellular cytokines were analyzed by gating on proliferating (CFSE^{low}) CD4$^+$ T cells after a 5-hour restimulation with phorbol 12-myristate 13-acetate (50 ng/mL, Sigma) and ionomycin (1 mg/mL, Sigma) in the presence of GolgiStop (BD Pharmingen). Cells were fixed, permeabilized (0.1% saponin in PBS 0.5% BSA), and stained with antibodies directed against mouse IL-4, IL-5, IL-13 or IFN-γ. Flow cytometric data were acquired on a BD FACSCanto cytometer and were analyzed using FlowJo software (Tree Star, Inc, Ashland, Ore).

Skin section preparation, histology, immunofluorescence, and confocal microscopy

Mouse back skin (1-2 cm^2) samples were fixed in 10% formalin and embedded in paraffin. Four-micrometer-thick sections were stained with H&E, and photographs were taken using a Nikon H600L microscope and analyzed with NIS-Elements imaging Software. All sections were “coded” so the evaluator was not aware of their identity, as previously described[8]. Eosinophils and neutrophils were counted on H&E-stained skin sections from all mouse strains. For immunostaining of mouse specimens, 4-μm-thick sections were pretreated using a heat-induced epitope retrieval method[8] in 10 mM sodium citrate buffer (pH 6.0), then permeabilized for 30 minutes in PBS supplemented with 0.5% BSA and 0.1% saponin. Permeabilized skin sections were incubated overnight at 4°C with primary antibodies, extensively washed, and incubated with appropriate secondary antibodies for 2 hours at room temperature in the dark. Images of 1024 x 1024 pixels were acquired using a Zeiss LSM780 and LSM710 Meta inverted confocal laser-scanning microscopes. Images were processed using Zen software (Zeiss). Epidermal K6, K17, Claudin 1, Filaggrin, Loricrin and E-cadherin mean fluorescence intensities were analyzed using the "measurement function" of ImageJ software on randomly chosen epidermal areas of identical size (i.e., same total number of pixels).

Amounts of serum *D. farinae*-specific IgG1 and IgE antibodies by ELISA

Each incubation step described below was followed by 3 to 5 washing steps using PBS containing 0.05% Tween-20. MaxiSorp ELISA plates (Nunc) were coated with 5 μg/ml *D. farinae* at 4°C overnight. Plates were then blocked with 1% Bovine Serum Albumin (BSA) in PBS for at least 2 hours at room temperature. Sera diluted in PBS containing 1% BSA were added and incubated in the blocked wells for 2 hours at 37°C. Afterwards, biotinylated detection antibodies (rat anti-mouse IgG1 and rat anti-mouse IgE; BD Biosciences; 1:1000) were then added for 1 hour at room temperature followed by incubation with horseradish peroxidase-conjugated streptavidin (BD Biosciences; 1:2000) for 30 minutes at room

temperature. Reaction was then revealed using supersensitive 3,3',5,5'-tetramethylbenzidine (TMB; Sigma Aldrich) substrate and OD was measured at 450 nm.

D. farinae proteolytic activity assay

D. farinae samples were diluted to 200 μg/mL in a reaction buffer composed of Sodium Phosphate 100 mM pH 6, EDTA 10 mM, and DTT 1 mM. The extract was incubated or not with irreversible protease inhibitors (cysteine protease inhibitor E64 100 nM or serine protease inhibitor AEBSF 1 mM) in a reaction volume of 50 μL. Activity was measured using Boc-Gln-Ala-Arg-AMC fluorogenic substrate (200 μM, diluted in the same reaction buffer). *D. farinae* extracts and substrate solutions were incubated separately for 20 minutes at 37°C. Immediately after addition of 50 μL substrate solution on the *D. farinae* extracts, the release of AMC fluorescence was followed over time using a varioskan Flash apparatus (Thermo Scientific). The initial velocity reflecting proteolytic activity was calculated from the kinetics curves. A control was performed by heat-inactivating *D. farinae* extract for 60 minutes at 95°C before addition of substrate. An additional control was performed in a reaction buffer devoid of DTT.

Dorsal Root Ganglia (DRG) dissociation, culture, and Ca^{2+} imaging

DRG neurons from all spinal levels were collected in ice-cold Dulbecco's modified Eagle's medium (DMEM)/F-12 supplemented with 10% FBS, penicillin (100 U/mL), and streptomycin (100 μg/mL). DRGs were digested with a mixture of dispase (5 mg/ml) and collagenase type I (1 mg/ml) enzyme at 37°C for 45 minutes. After dissociation, cells were spun at 300*g* and re-suspended in media before being plated on glass coverslips coated with poly-D-lysine (0.5 mg/ml) and laminin (10 μg/ml, Invitrogen) or Lab-tek II chambers slide with cover (Thermo Fisher Scientific). DRGs were cultured in media supplemented with 50 ng/mL NGF at 37°C overnight (12-24 hours) before experimentation. In some experiments, control peptide, or MyD88 inhibitory peptide (100 μM), were added to the DRG cultures for 16 h. Cells were imaged in calcium imaging buffer (CIB; 10 mM HEPES, 1.2 mM $NaHCO_3$, 130 mM NaCl, 3 mM KCl, 2.5 mM $CaCl_2$, 0.6 mM $MgCl_2$, 20 mM glucose, and 20 mM sucrose at pH 7.4 and 290-300 mOsm) or HBSS. To monitor changes in intracellular [Ca^{2+}] ($[Ca^{2+}]_i$), cells were loaded with Fura2-AM or Fluo-4 for 30 minutes in the dark at 37°C in CIB or Hepes /HBSS just prior to imaging. Emission at 520 nm was monitored after excitation at 340 nm (Ca^{2+} bound) or 380 (unbound). Cells were imaged for 20 seconds to establish a baseline before compounds were added. DRG were stimulated with 5 ng/ml *D. farina*e, 5 ng/ml heat-treated *D. farina*e (95°C for 60 minutes), 5 ng/ml *D. farina*e treated with 2.5 pM E64, 37°C for 30 minutes), 5 ng/ml SEB or 1 μM capsaicin. At the end of every imaging trial, 50 mM KCl was added as a positive control. Cells were identified as responding if the intracellular [Ca^{2+}] rose by either 50% compared to baseline or 50% compared to the $[Ca^{2+}]_i$ change assayed during addition of 50 mM KCl (neurons only). Damaged, detached, high-baseline and motion-activated cells were excluded from analyses. Those experiments were performed in the Dong Lab at Johns Hopkins University (and confirmed in the Gaudenzio Lab at INSERM, Toulouse France) in compliance with Johns Hopkins University ethical guidelines and Inserm Toulouse guidelines.

Quantification of SP secretion

DRG of mice were cultured as described above, rinsed in Hanks Balanced Salt Solution (HBSS; Sigma), and incubated in L-cysteine containing 1% Papain (Sigma) for 10 minutes at 37°C. After a wash with filtered Leibovitz's L-15 Medium (Gibco) containing 10% FBS (Sigma), they were incubated in HBSS containing collagenase (1 mg/ml; Sigma) and dispase (4 mg/ml, Sigma) at 37°C for 10 min. After titration, cells were plated in a Poly-D-lysine-laminin (Sigma)-coated 12 well-plate (Corning) and recovered with the complete culture media (DMEM-Glutamax, 2.5% FBS, 1% pen/strep and ARAC, FUDR, uridine – 10 μM each; all from Sigma). Cells were incubated for 5 minutes with vehicle or 5 ng/ml *D. farinae* or 5 ng/ml SEB or and 125 nM capsaicin. Cell supernatants were tested with a Substance P Elisa kit (Enzo) following the manufacturer's recommendations.

Ear pinna injection, mast cell staining, and ear thickness measurement

8 μg of Av.SRho in 20 μl of PBS were injected i.d. into both ear pinnae of WT, *Mrgprb2*$^{mut/mut}$, and RTX-treated mice, and the respective *Mrgprb2*$^{+/+}$ or DMSO-treated control mice, to selectively label mast cell secretory granules *in vivo*, as previously described[37]. 7 days later, ear thickness was measured and then right ear pinnae were injected i.d. with 1 μg *D. farinae* + 50 ng SEB (pre-incubated or not for 30 minutes at 37°C with 100 nM of E64 cysteine protease inhibitor) or 1 μM capsaicin in 20 μl PBS. In some experiments, ear pinnae were injected i.d. with 1 μg *D. farinae* + 50 ng SEB with 15 μg of IgG anti-SP (Sigma Aldrich) in 20 μl PBS. Left ear pinnae were injected with 20 μL of respective control solutions: vehicle alone or in combination with IgG isotype control. 45 minutes later, ear thickness was measured again and mice were euthanized before ear excision. Whole ears were fixed in 4% paraformaldehyde (PFA) overnight, then mounted on microscopy slides and placed under a LSM710 Meta inverted confocal laser-scanning microscope. High resolution Z-stack images 1024 x 1024 pixels of Av.SRho fluorescent signal were acquired using a 20x objective. Images were then processed using Image J and Imaris (Bitplane) softwares.

In vivo two-photon microscopy of living mice

Experiments were conducted as previously described[25,37]. Briefly, 8 μg of Av.SRho in 20 μl of PBS were injected i.d. into the ear pinna of Pirt-GCaMP3 mice. 1 week later, mice were injected i.d. with vehicle, 1 μM capsaicin, or 1 μg *D. farinae* and 50 ng SEB (used alone or in combination) in a final volume of 20 μl then placed under the two-photon microscope on a custom-built 3-D printed mouse platform; anesthesia was maintained by a mixture of Isoflurane/O2 and the animal's ear pinna was kept at 36°C using a heating pad system. The fluorescence corresponding to Av.SRho^{+} mast cell granule structures or GCaMP3^{+} skin neurons was measured using a Prairie Ultima IV two-photon microscope (Spectra Physics Mai Tai HP Ti:sapphire laser, tunable from 690 to 1040 nm). Images were acquired in 3-D up to 100-150 μm depth, with 20x Olympus XLUM Plan Fl N.A. 0.95 water-immersion objective and a software zoom setting of 1 or 3 (8 bits/pixel 1024x1024, scaling x= 0.228 μm, y= 0.228 μm, z= 0.5−μm). Modeling and analysis of fluorescent signals were performed using untreated image sequences, as previously described[25], using Imaris software (Bitplane) and Image J software version Fiji, respectively.

Automated computational analysis of the minimum distance between mast cells and neurons in the dermis of living mice

1) 3D high resolution images were taken using a Prairie Ultima IV two-photon microscope as described above. The following steps have been automated in the software Imaris Bitplane version 9.2. 2) Hair follicles' autofluorescent signals were modeled into matched 3D objects using the isosurface algorithm. 3) Autofluorescent signals corresponding to the generated isosurfaces were depleted from the GCaMP3 fluorescence detection channel so that the hair follicles were no longer detectable in that particular channel. 4) The filament tracer algorithm was applied in the GCaMP3 fluorescence detection channel in order to precisely trace the trajectories and exact shapes of GCaMP3 fluorescent signals. Filament traces were then converted into fluorescent signals in a new fluorescent channel. 5) Those newly generated fluorescent signals were modeled into matched 3D objects using the isosurface algorithm. The distance transformation algorithm was applied to those new isosurfaces resulting in the generation of a new distance transformation channel. 6) Av.SRho fluorescent signals were modeled into matched 3D objects using the isosurface algorithm. The intensity minimum (i.e., distance minimum in μm) to the distance transformation channel (i.e., modeled sensory neurons) was calculated for each of the Av.SRho$^+$ isosurfaces of at least 5 μm of diameter (corresponding to Av.SRho$^+$ mast cell cellular bodies and excluding small exteriorized Av.SRho$^+$ granules structures). 7) Results per field of view were generated into separated Excel sheets. The exact same procedure was automatically applied to all analyzed 3D images.

Statistics

Statistical tests were performed with the software Prism 6 (GraphPad Software). Two-tailed unpaired/paired Student's *t* tests, 1-way ANOVA with Tukey's test for multiple comparisons or Holm-Sidak's post-hoc test were performed on samples as noted in the respective figure legends. A *P* value of less than 0.05 was considered statistically significant.

Supplementary Material

Refer to Web version on PubMed Central for supplementary material.

Acknowledgements

We thank all members of the Galli and Gaudenzio laboratories for discussions, and C. Liu for technical assistance. We thank A. Olson and the Stanford Neuroscience Microscopy Service (supported by NIH NS069375); this article is solely the responsibility of the authors and does not necessarily represent the official views of the NCRR or the NIH), F. L'Faqihi (IFR30, Plateau Technique Cytometrie, Toulouse) and S. Allart (IFR30, Plateau Technique Imagerie Cellulaire, Toulouse) for technical assistance. T.M. is a Research Associate of the F.R.S.-FNRS and is supported by an "Incentive Grant for Scientific Research" of the F.R.S.-FNRS (F.4508.18), by the FRFS-WELBIO under grant CR-2017s-04, the Acteria Foundation and an ERC Starting Grant (IM-ID 801823); P.S. acknowledges support from and the Austrian Science Fund (FWF): P31113-B30; L.L.R. acknowledges support from the European Commission (Marie Skłodowska-Curie Individual Fellowship H2020-MSCA-IF-2014 656086) and the INSERM ATIP-Avenir program. This work was supported by grants from NIH (S.J. Galli: Grants U19 AI104209, R01 AR067145, and R01 AI32494), the United States-Israel Binational Science Foundation (Grant 2013263), and the Sean N. Parker Center for Allergy and Asthma Research, Stanford University (to S.J. Galli); the Société Française de Dermatologie (SFD), the Société Française d'Allergologie (SFA), the Marie Skłodowska-Curie Individual Fellowship (H2020-MSCA-IF-2016 #749629), the European Research Council (ERC-2018-STG #802041) and the INSERM ATIP-Avenir program (to N. Gaudenzio).

References

1. Zheng T, Yu J, Oh MH, Zhu Z. The atopic march: progression from atopic dermatitis to allergic rhinitis and asthma. Allergy Asthma Immunol Res. 2011; 3:67–73. DOI: 10.4168/aair.2011.3.2.67 [PubMed: 21461244]
2. Leung DY, Bieber T. Atopic dermatitis. Lancet. 2003; 361:151–160. DOI: 10.1016/S0140-6736(03)12193-9 [PubMed: 12531593]
3. Sager N, Feldmann A, Schilling G, Kreitsch P, Neumann C. House dust mite-specific T cells in the skin of subjects with atopic dermatitis: frequency and lymphokine profile in the allergen patch test. J Allergy Clin Immunol. 1992; 89:801–810. [PubMed: 1373161]
4. Langer K, Breuer K, Kapp A, Werfel T. Staphylococcus aureus-derived enterotoxins enhance house dust mite-induced patch test reactions in atopic dermatitis. Exp Dermatol. 2007; 16:124–129. DOI: 10.1111/j.1600-0625.2006.00523.x [PubMed: 17222226]
5. Park HY, et al. Staphylococcus aureus Colonization in Acute and Chronic Skin Lesions of Patients with Atopic Dermatitis. Ann Dermatol. 2013; 25:410–416. DOI: 10.5021/ad.2013.25.4.410 [PubMed: 24371386]
6. Bunikowski R, et al. Evidence for a disease-promoting effect of Staphylococcus aureus-derived exotoxins in atopic dermatitis. J Allergy Clin Immunol. 2000; 105:814–819. DOI: 10.1067/mai.2000.105528 [PubMed: 10756234]
7. McFadden JP, Noble WC, Camp RD. Superantigenic exotoxin-secreting potential of staphylococci isolated from atopic eczematous skin. Br J Dermatol. 1993; 128:631–632. [PubMed: 8338746]
8. Marichal T, et al. Guanine nucleotide exchange factor RABGEF1 regulates keratinocyte-intrinsic signaling to maintain skin homeostasis. J Clin Invest. 2016; 126:4497–4515. DOI: 10.1172/JCI86359 [PubMed: 27820702]
9. Cookson W. The immunogenetics of asthma and eczema: a new focus on the epithelium. Nat Rev Immunol. 2004; 4:978–988. DOI: 10.1038/nri1500 [PubMed: 15573132]
10. Holgate ST. The epithelium takes centre stage in asthma and atopic dermatitis. Trends Immunol. 2007; 28:248–251. DOI: 10.1016/j.it.2007.04.007 [PubMed: 17466594]
11. Palmer CN, et al. Common loss-of-function variants of the epidermal barrier protein filaggrin are a major predisposing factor for atopic dermatitis. Nature genetics. 2006; 38:441–446. DOI: 10.1038/ng1767 [PubMed: 16550169]
12. O'Regan GM, Sandilands A, McLean WH, Irvine AD. Filaggrin in atopic dermatitis. J Allergy Clin Immunol. 2008; 122:689–693. DOI: 10.1016/j.jaci.2008.08.002 [PubMed: 18774165]
13. Oyoshi MK, He R, Kumar L, Yoon J, Geha RS. Cellular and molecular mechanisms in atopic dermatitis. Adv Immunol. 2009; 102:135–226. DOI: 10.1016/S0065-2776(09)01203-6 [PubMed: 19477321]
14. LaMotte RH, Dong X, Ringkamp M. Sensory neurons and circuits mediating itch. Nature reviews. Neuroscience. 2014; 15:19–31. DOI: 10.1038/nrn3641 [PubMed: 24356071]
15. Salomon J, Baran E. The role of selected neuropeptides in pathogenesis of atopic dermatitis. Journal of the European Academy of Dermatology and Venereology : JEADV. 2008; 22:223–228. DOI: 10.1111/j.1468-3083.2007.02399.x [PubMed: 18211417]
16. Toyoda M, et al. Nerve growth factor and substance P are useful plasma markers of disease activity in atopic dermatitis. Br J Dermatol. 2002; 147:71–79. [PubMed: 12100187]
17. Riol-Blanco L, et al. Nociceptive sensory neurons drive interleukin-23-mediated psoriasiform skin inflammation. Nature. 2014; 510:157–161. DOI: 10.1038/nature13199 [PubMed: 24759321]
18. Kashem SW, et al. Nociceptive Sensory Fibers Drive Interleukin-23 Production from CD301b+ Dermal Dendritic Cells and Drive Protective Cutaneous Immunity. Immunity. 2015; 43:515–526. DOI: 10.1016/j.immuni.2015.08.016 [PubMed: 26377898]
19. Cardoso V, et al. Neuronal regulation of type 2 innate lymphoid cells via neuromedin U. Nature. 2017; 549:277–281. DOI: 10.1038/nature23469 [PubMed: 28869974]
20. Baral P, et al. Nociceptor sensory neurons suppress neutrophil and gammadelta T cell responses in bacterial lung infections and lethal pneumonia. Nat Med. 2018; 24:417–426. DOI: 10.1038/nm.4501 [PubMed: 29505031]

21. Moriyama S, et al. beta2-adrenergic receptor-mediated negative regulation of group 2 innate lymphoid cell responses. Science. 2018; 359:1056–1061. DOI: 10.1126/science.aan4829 [PubMed: 29496881]
22. Wallrapp A, et al. Erratum: The neuropeptide NMU amplifies ILC2-driven allergic lung inflammation. Nature. 2017; 551:658.doi: 10.1038/nature24480
23. Hofmann AM, Abraham SN. New roles for mast cells in modulating allergic reactions and immunity against pathogens. Curr Opin Immunol. 2009; 21:679–686. [PubMed: 19828301]
24. McNeil BD, et al. Identification of a mast-cell-specific receptor crucial for pseudo-allergic drug reactions. Nature. 2014; 519:237–241. DOI: 10.1038/nature14022 [PubMed: 25517090]
25. Gaudenzio N, et al. Different activation signals induce distinct mast cell degranulation strategies. J Clin Invest. 2016; 126:3981–3998. DOI: 10.1172/JCI85538 [PubMed: 27643442]
26. Monti G, Tonetto P, Mostert M, Oggero R. Staphylococcus aureus skin colonization in infants with atopic dermatitis. Dermatology. 1996; 193:83–87. [PubMed: 8884140]
27. Ando T, et al. Mast cells are required for full expression of allergen/SEB-induced skin inflammation. J Invest Dermatol. 2013; 133:2695–2705. DOI: 10.1038/jid.2013.250 [PubMed: 23752044]
28. Beck LA, et al. Dupilumab treatment in adults with moderate-to-severe atopic dermatitis. N Engl J Med. 2014; 371:130–139. DOI: 10.1056/NEJMoa1314768 [PubMed: 25006719]
29. Usoskin D, et al. Unbiased classification of sensory neuron types by large-scale single-cell RNA sequencing. Nature neuroscience. 2015; 18:145–153. DOI: 10.1038/nn.3881 [PubMed: 25420068]
30. Lattin JE, et al. Expression analysis of G Protein-Coupled Receptors in mouse macrophages. Immunome research. 2008; 4:5.doi: 10.1186/1745-7580-4-5 [PubMed: 18442421]
31. Reithofer M, Jahn-Schmid B. Allergens with Protease Activity from House Dust Mites. Int J Mol Sci. 2017; 18doi: 10.3390/ijms18071368
32. Hammad H, Lambrecht BN. Barrier Epithelial Cells and the Control of Type 2 Immunity. Immunity. 2015; 43:29–40. DOI: 10.1016/j.immuni.2015.07.007 [PubMed: 26200011]
33. Locksley RM. Asthma and allergic inflammation. Cell. 2010; 140:777–783. DOI: 10.1016/j.cell.2010.03.004 [PubMed: 20303868]
34. Palm NW, Rosenstein RK, Medzhitov R. Allergic host defences. Nature. 2012; 484:465–472. DOI: 10.1038/nature11047 [PubMed: 22538607]
35. Stewart GA, Thompson PJ. The biochemistry of common aeroallergens. Clin Exp Allergy. 1996; 26:1020–1044. [PubMed: 8889258]
36. Cayrol C, et al. Environmental allergens induce allergic inflammation through proteolytic maturation of IL-33. Nat Immunol. 2018; 19:375–385. DOI: 10.1038/s41590-018-0067-5 [PubMed: 29556000]
37. Reber LL, et al. Imaging protective mast cells in living mice during severe contact hypersensitivity. JCI Insight. 2017; 2:e92900.doi: 10.1172/jci.insight.92900
38. Kim YS, et al. Central terminal sensitization of TRPV1 by descending serotonergic facilitation modulates chronic pain. Neuron. 2014; 81:873–887. DOI: 10.1016/j.neuron.2013.12.011 [PubMed: 24462040]
39. Lansu K, et al. In silico design of novel probes for the atypical opioid receptor MRGPRX2. Nat Chem Biol. 2017; 13:529–536. DOI: 10.1038/nchembio.2334 [PubMed: 28288109]
40. Alving K, et al. Association between histamine-containing mast cells and sensory nerves in the skin and airways of control and capsaicin-treated pigs. Cell and tissue research. 1991; 264:529–538. [PubMed: 1714354]
41. Barbara G, et al. Activated mast cells in proximity to colonic nerves correlate with abdominal pain in irritable bowel syndrome. Gastroenterology. 2004; 126:693–702. [PubMed: 14988823]
42. Hagiyama M, et al. Increased expression of cell adhesion molecule 1 by mast cells as a cause of enhanced nerve-mast cell interaction in a hapten-induced mouse model of atopic dermatitis. Br J Dermatol. 2013; 168:771–778. DOI: 10.1111/bjd.12108 [PubMed: 23106683]
43. Pang X, Boucher W, Triadafilopoulos G, Sant GR, Theoharides TC. Mast cell and substance P-positive nerve involvement in a patient with both irritable bowel syndrome and interstitial cystitis. Urology. 1996; 47:436–438. DOI: 10.1016/S0090-4295(99)80469-5 [PubMed: 8633418]

44. Suzuki R, et al. Direct neurite-mast cell communication in vitro occurs via the neuropeptide substance P. J Immunol. 1999; 163:2410–2415. [PubMed: 10452975]
45. Buhner S, et al. Calcium Imaging of Nerve-Mast Cell Signaling in the Human Intestine. Front Physiol. 2017; 8:971.doi: 10.3389/fphys.2017.00971 [PubMed: 29238306]
46. Green DP, Limjunyawong N, Gour N, Pundir P, Dong X. A Mast-Cell-Specific Receptor Mediates Neurogenic Inflammation and Pain. Neuron. 2019; 101:412–420 e413. DOI: 10.1016/j.neuron.2019.01.012 [PubMed: 30686732]
47. Meixiong J, et al. Activation of Mast-Cell-Expressed Mas-Related G-Protein-Coupled Receptors Drives Non-histaminergic Itch. Immunity. 2019; 50:1163–1171 e1165. DOI: 10.1016/j.immuni.2019.03.013 [PubMed: 31027996]
48. Vocanson M, Hennino A, Rozieres A, Poyet G, Nicolas JF. Effector and regulatory mechanisms in allergic contact dermatitis. Allergy. 2009; 64:1699–1714. DOI: 10.1111/j.1398-9995.2009.02082.x [PubMed: 19839974]
49. Che D, et al. Mivacurium induce mast cell activation and pseudo-allergic reactions via MAS-related G protein coupled receptor-X2. Cell Immunol. 2018; 332:121–128. DOI: 10.1016/j.cellimm.2018.08.005 [PubMed: 30121125]
50. Takamori A, et al. Identification of inhibitory mechanisms in pseudo-allergy involving Mrgprb2/MRGPRX2-mediated mast cell activation. J Allergy Clin Immunol. 2019; 143:1231–1235 e1212. DOI: 10.1016/j.jaci.2018.10.034 [PubMed: 30414859]

Europe PMC Funders Author Manuscripts

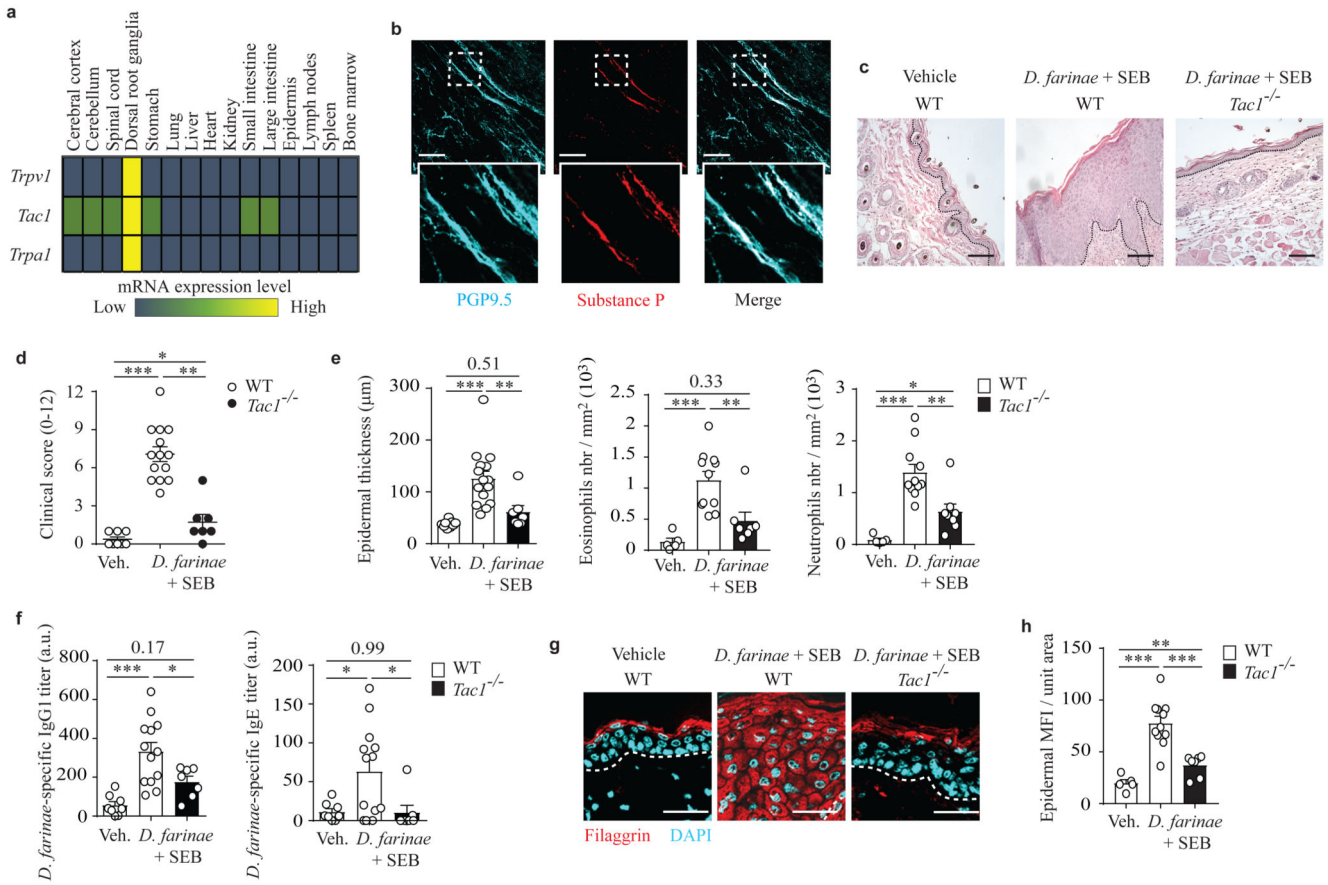

Figure 1. *Tac1* gene expression is required for the full development of pathological features in a model of allergic skin inflammation.

a, Publicly available microarray gene expression data of *Trpv1*, *Tac1* and *Trpa1* in different mouse tissues (GSE 10246); data are shown using a heat map of mRNA expression levels. **b,** Representative 3D confocal microscopy picture of whole-mounted normal back skin stained for PGP9.5 (a pan neuronal marker, cyan) and substance P (red). **c**, Representative hematoxylin & eosin (H&E) staining of vehicle- or *D. farinae* + SEB-treated areas in WT or *Tac1*$^{-/-}$ mice. **d**, Clinical scores (0-12) of vehicle- or *D. farinae* + SEB-treated areas in WT or *Tac1*$^{-/-}$ mice treated as in **c**. **e**, Epidermal thickness (µm) (left), number of eosinophils (middle) and neutrophils (right) in skin sections in WT or *Tac1*$^{-/-}$ mice treated as in **c**. **f**, Serum levels (arbitrary unit [a.u]) of *D. farinae*-specific IgG1 (left) and IgE (right) antibodies in vehicle- or *D. farinae* + SEB-treated WT or *Tac1*$^{-/-}$ mice as in **c**. **g,h,** Representative confocal microscopy pictures of back skin sections (**g**) and fluorescence analysis (**h**) of filaggrin staining in the epidermis of vehicle- or *D. farinae* + SEB-treated areas in WT or *Tac1*$^{-/-}$ mice treated as in **c**. Bars = 100 µm, dotted black (**c**) or white (**g**) lines indicate the junction epidermis/dermis. Each circle = one mouse. Number of mice: (**b**) n = 3; (**c-h**) n = 6 (WT Vehicle), n = 14 (WT *D. farinae* + SEB), n = 7 (*Tac1*$^{-/-}$). (**e**,**f**,**h**) Open bars: WT mice; black bars: *Tac1*$^{-/-}$ mice. (**b-h**) Data from three independent experiments, mean ± SEM (**d**), mean + SEM (**e**,**f**,**h**); 1-way ANOVA with Tukey's test for multiple comparisons, *P<.05 **P<.01 ***P<.001.

Europe PMC Funders Author Manuscripts

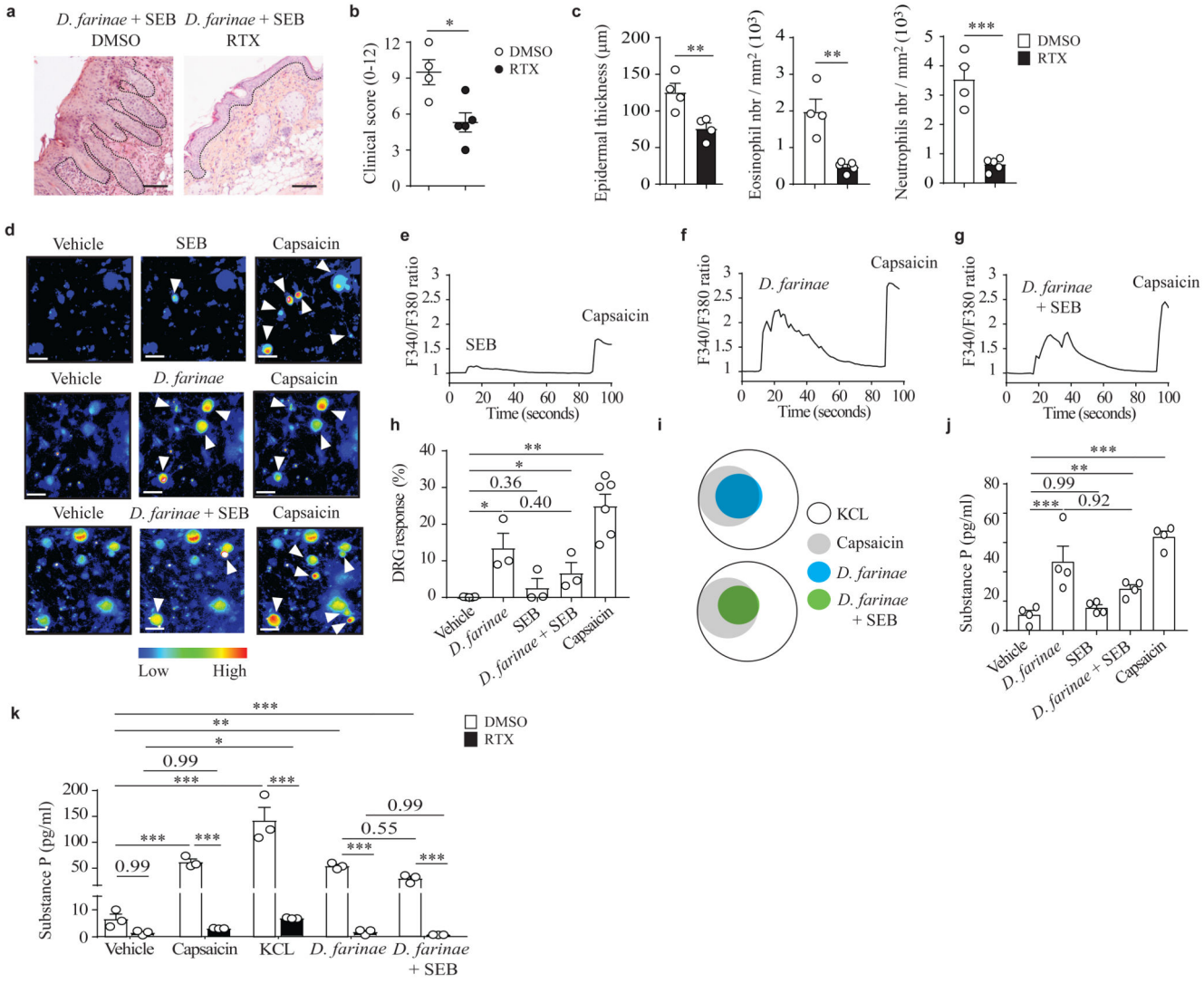

Figure 2. TRPV1$^+$ nociceptors are required for the full development of allergic skin inflammation and *D. farinae* extracts directly induce neuronal activation.

a, Representative H&E staining of *D. farinae* + SEB-treated areas in mock (dimethylsulphoxide [DMSO])-treated or RTX-treated (TRPV1$^+$ nociceptor ablated) mice. **b**, Clinical scores (0-12) of *D. farinae* + SEB-treated areas in DMSO- or RTX-treated mice as in **a**. **c**, Epidermal thickness (µm) (left), number of eosinophils (middle) and neutrophils (right) of *D. farinae* + SEB-treated areas in DMSO- or RTX-treated mice as in **a**. Number of mice: (**a-c**) n = 4 (DMSO) and n = 5 (RTX); data are from two independent experiments; mean + SEM, two-tailed, unpaired t-test, *P<.05 **P<.01 ***P<.001. **d-h**, Representative Fura-2 ratiometric fields (**d**), associated calcium traces (**e-g**) and (**h**) proportion of responding DRG neurons (%) of *ex vivo* cultured DRG neurons (expressed as % of DRG neurons responding to 50 mM KCL) stimulated with 5 ng/ml SEB (top **d**,**e**,**h**) or 5 ng/ml *D. farinae* (middle **d**,**f**,**h**) or both (bottom **d**,**g**,**h**) and 1 µM capsaicin (**d-h**). (**d**) Bars = 50 µm, white arrow heads indicate neurons with increased Fura-2 fluorescence. (**d-h**) Data are from three independent experiments performed with DRGs from n = 3 (for the condition of

Europe PMC Funders Author Manuscripts

vehicle-, *D. farinae*, SEB or *D. farinae* + SEB-treated DRG neurons) and n = 6 (for the condition of capsaicin-treated DRG neurons) different mice; mean + SEM, two-tailed, unpaired t-test, *P<.05 **P<.01. **i**, Venn diagrams of responding DRG neurons. **j,k,** Substance P secretion in DRG neurons cultured *ex vivo* from (**j**) WT mice, (**k**) DMSO (open bars)- versus RTX (black bars)-treated mice and stimulated as indicated. Data are from (**j**) 4 and (**k**) 3 independent experiments, mean + SEM, two-tailed, unpaired t-test, *P<.05 **P<.01 ***P<.001. Each circle = one mouse.

Europe PMC Funders Author Manuscripts

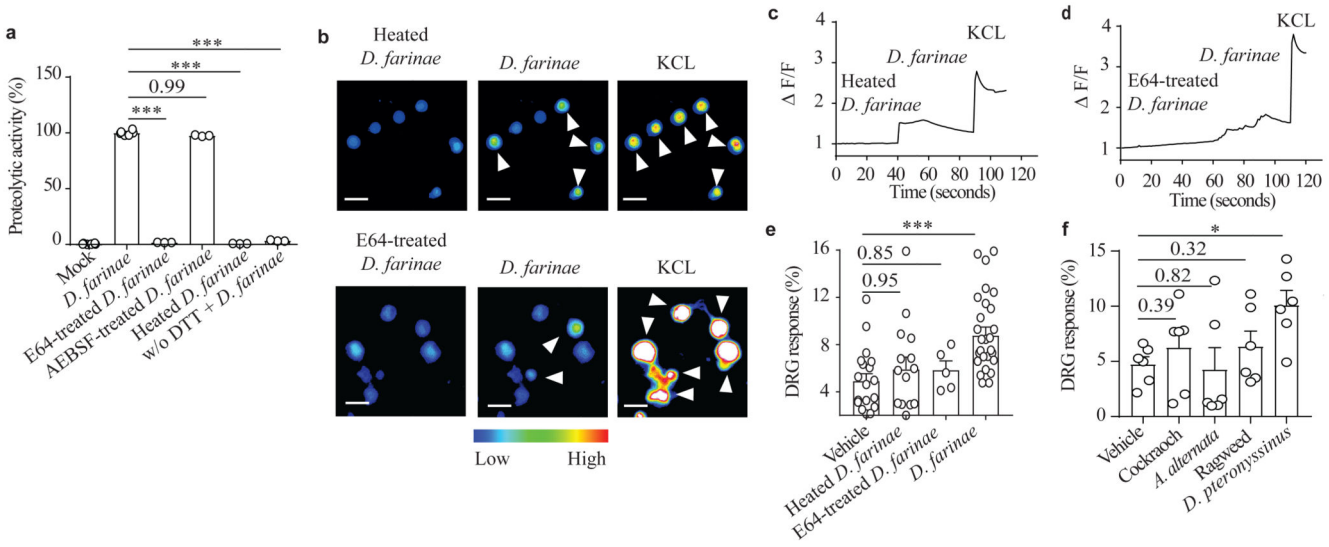

Figure 3. Activation of DRG neurons by *D. farinae* extract depends on cysteine protease activity.

a, Protease activity in *D. farinae* extracts heat inactivated at 95°C for 60 minutes (Heated), or treated with cysteine- (E64, 100 nM) or serine- (AEBSF, 1 mM) protease inhibitors, with or without dithiothreitol (DTT). Data are from three independent experiments performed with three independent biological samples, mean + SEM, One way ANOVA and Holm-Sidak's post- hoc test, *** P<.001. **b-e**, Representative Fura-2 ratiometric fields (**b**), associated calcium traces (**c,d**) and (**e**) proportion of responding DRG neurons (%) in *ex vivo* cultured DRG neurons (expressed as % of DRG neurons responding to 50 mM KCL) stimulated sequentially with 5 ng/ml heated *D. farinae* (top **b,c**) or 5 ng/ml E64 (2.5 pM)-treated *D. farinae* (bottom **b**,**d**), 5 ng/ml *D. farinae* and 50 mM KCL. Data are from five independent experiments performed with 22 (for the conditions Vehicle and *D. farinae*), 14 (for the condition Heated *D. farinae*) and 5 (for the condition E64-treated *D. farinae*) independent experiments performed with independent biological samples, mean + SEM, two-tailed, unpaired t-test, ***P<.001. **f**, Proportion of responding DRG neurons stimulated with either Vehicle, 5 ng/ml *D. pteronyssinus,* 5 ng/ml German cockroach, 5 ng/ml *A. alternata*, or 5 ng/ml ragweed expressed as % of DRG neurons responding to 50 mM KCL. Data are from six independent experiments performed with six independent biological samples, mean + SEM, two-tailed, unpaired *t*-test, *P<.05. Each circle = one mouse.

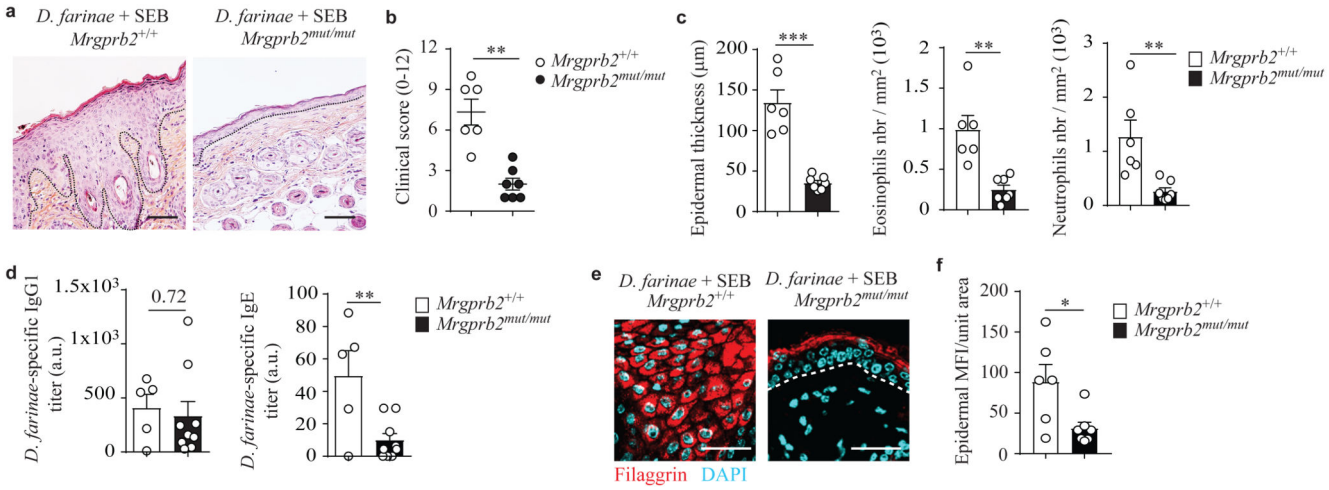

Figure 4. Genetic inactivation of MRGPRB2 largely prevents development of pathology in a model of allergic skin inflammation.

a, Representative H&E staining of *D. farinae* + SEB-treated areas in *Mrgprb2*$^{mut/mut}$ and *Mrgprb2*$^{+/+}$ mice; dotted black lines indicate the junction epidermis/dermis. **b**, Clinical scores (0-12) of *D. farinae* + SEB-treated areas in *Mrgprb2*$^{mut/mut}$ and *Mrgprb2*$^{+/+}$ mice as in **a**. **c**, Epidermal thickness (µm) (left), number of eosinophils (middle) and neutrophils (right) in *D. farinae* + SEB-treated areas in *Mrgprb2*$^{mut/mut}$ and *Mrgprb2*$^{+/+}$ mice treated as in **a**. **d**, Serum levels (arbitrary unit [a.u]) of *D. farinae*-specific IgG1 (left) and IgE (right) antibodies of *D. farinae* + SEB-treated *Mrgprb2*$^{mut/mut}$ and *Mrgprb2*$^{+/+}$ mice as in **a**. **e,f,** Representative confocal microscopy of back skin section (**e**) and fluorescence analysis (**f**) of filaggrin staining of *D. farinae* + SEB-treated areas in *Mrgprb2*$^{mut/mut}$ and *Mrgprb2*$^{+/+}$ mice as in **a**. White lines indicate the junction epidermis/dermis. Bars = 100 µm. Each open circle = one mouse. Number of mice: (**a-c,e,f**) n = 6 (*Mrgprb2*$^{+/+}$), n = 7 (*Mrgprb2*$^{mut/mut}$); (**d**) n = 5 (*Mrgprb2*$^{+/+}$), n = 9 (*Mrgprb2*$^{mut/mut}$). Mean ± SEM (**b**), mean + SEM (**c,d,f**), two-tailed, unpaired *t*-test, *P<.05 **P<.01 ***P<.001.

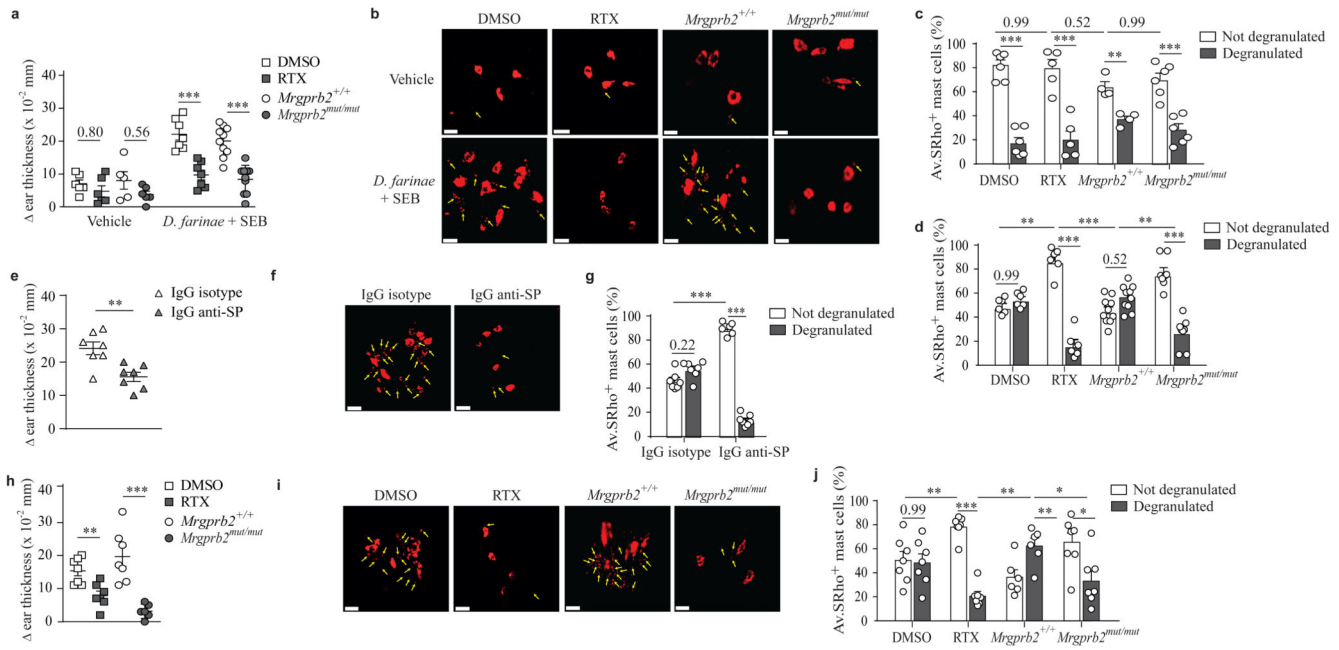

Figure 5. Sensory neurons, MRGPRB2 and substance P are required to trigger *in vivo* mast cell degranulation and associated skin swelling in response to *D. farinae* and SEB antigens.

a, Changes (Δ) in ear thickness 45 minutes after i.d. injection of vehicle or *D. farinae* + SEB in DMSO-treated (open squares), RTX-treated (grey squares), *Mrgprb2*$^{+/+}$ (open circles) or *Mrgprb2*$^{mu/mut}$ (grey circles) mice. **b**, 3D representative confocal microscopy pictures of Av.SRho fluorescent signal (red) in whole-mounted ears in mice treated as in **a**. **c**, Quantification of not degranulated (i.e., lacking exteriorized granules, white bars) or degranulated mast cells (i.e., presence of exteriorized Av.SRho^{+} granule structures, indicated with yellow arrows in **b** and grey bars) in DMSO-treated, RTX-treated, *Mrgprb2*$^{+/+}$ or *Mrgprb2*$^{mu/mut}$ mice 45 minutes after i.d. injection of vehicle. **d**, Same experiment as in **c** but 45 minutes after i.d. injection of *D. farinae* + SEB. **e**, Changes (Δ) in ear thickness 45 minutes after i.d. injection of *D. farinae* + SEB with IgG control isotype (open triangles) or with IgG anti-SP (grey triangles) in WT mice. **f,** 3D representative confocal microscopy pictures of Av.SRho fluorescent signal (red) in whole-mounted ears in mice treated as in **e**. g, Quantification of not degranulated or degranulated mast cells in mice treated as in **e**. **h**, Same experiment as in **a** but 45 after i.d. injection of capsaicin. **i**. Same experiment as in **b** but 45 after i.d. injection of capsaicin. **j**, Same experiment as in **d** but 45 after i.d. injection of capsaicin. Bars = 20 μm. All data are from two independent experiments with the following number of mice: (**a-d**) n = 6 (DMSO Vehicle), n = 5 (RTX Vehicle), n = 5 (*Mrgprb2*$^{+/+}$ Vehicle), n = 6 (*Mrgprb2*$^{mut/mut}$ Vehicle), n = 7 (DMSO *D. farinae* + SEB), n = 7 (RTX *D. farinae* + SEB), n = 9 (*Mrgprb2*$^{+/+}$ *D. farinae* + SEB), n = 9 (*Mrgprb2*$^{mut/mut}$ *D. farinae* + SEB); (**e-g**) n = 7 (IgG control isotype), n = 7 (IgG anti-SP); (**h-j**) n = 7 (DMSO), n = 7 (RTX), n = 7 (*Mrgprb2*$^{+/+}$), n = 7 (*Mrgprb2*$^{mut/mut}$). Mean ± SEM (**a,e,h**), mean + SEM (**c,d,g,j**), two-tailed, unpaired t-test, *P<.05 **P<.01 ***P<.001.

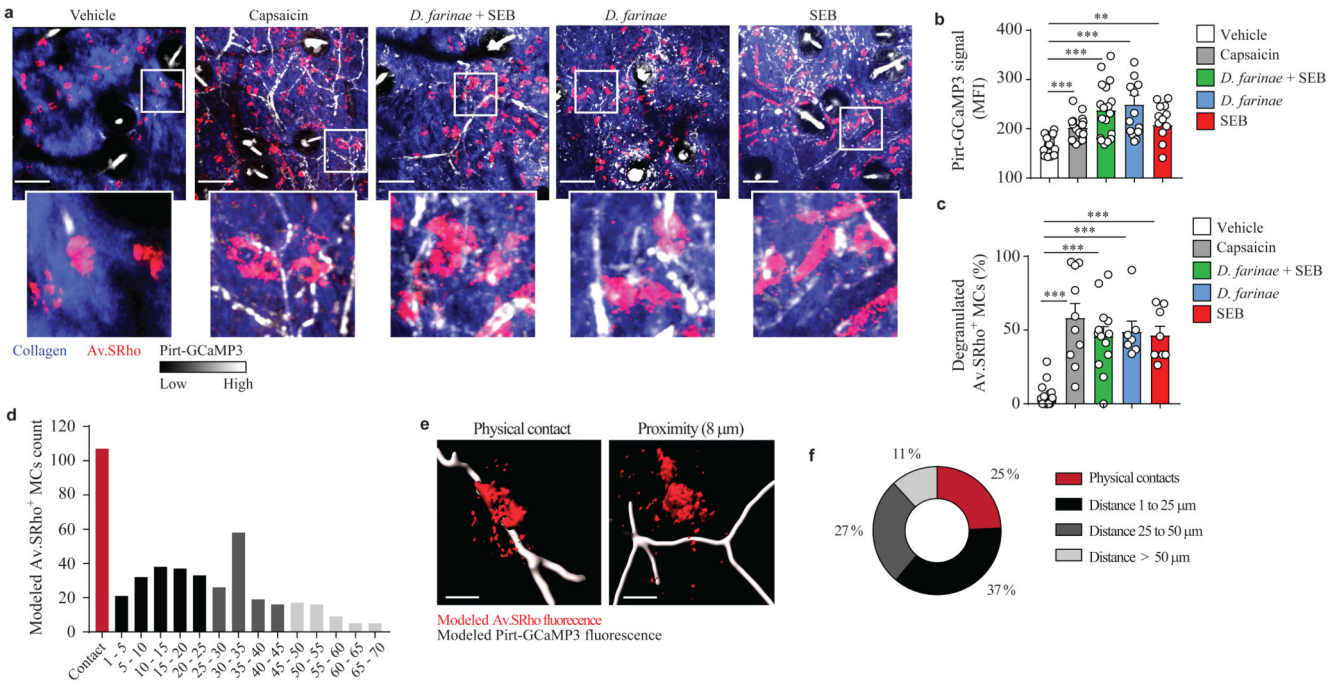

Figure 6. Dermal mast cells and TPRV1$^+$ nociceptors form sensory clusters in the skin that respond to *D. farinae* and SEB.

a, Representative high-resolution 3-D images of the dermis; merged fluorescence of Av.SRho (red), GCaMP3 calcium tracer (pseudocolor intensity scale) and collagen structures (blue) in Av.SRho-labeled ear pinna of Pirt-GCaMP3 mice 30-60 minutes after i.d. injection of vehicle or 1 µM capsaicin or 1 µg *D. farinae* and 50 ng SEB (alone or in combination). White lines identify magnified areas shown in lower images. Bars = 100 µm. **b**, Mean Fluorescence Intensity (MFI) of GCaMP3 fluorescent signal per field of view in mice treated as in **a**. **c**, Proportion (%) of Av.SRho$^+$ mast cells with exteriorized granule structures (i.e., activated to degranulate) per field of view in mice treated as in **a**. One symbol = one field analyzed. (**a-c**) All data are from three independent experiments with the following number of mice: n = 4 (vehicle), n = 5 (capsaicin), n = 5 (*D. farinae*), n = 3 (SEB), n = 5 (*D. farinae* + SEB). Mean + SEM, two-tailed, unpaired *t*-test, **P<.01 ***P<.001. **d**, Automated computational analysis of the minimum distance between modeled Av.SRho$^+$ mast cell bodies detected and modeled capsaicin-activated TRPV1$^+$ Pirt-GCaMP3$^+$ sensory neurons. **e**, Examples of modeled Av.SRho$^+$ mast cell bodies forming physical contact with (left) or in proximity to (right) modeled capsaicin-activated TRPV1$^+$ Pirt-GCaMP3$^+$ sensory neurons. **f**, Proportion (%) of 453 modeled Av.SRho$^+$ mast cell bodies from the ear pinnae of 3 different mice in physical contact with (red), at 1 to 25 µm (black), at 25 to 50 µm (dark grey) or at more than 50 µm (light grey) from modeled capsaicin-activated TRPV1$^+$ Pirt-GCaMP3$^+$ sensory neurons.

Europe PMC Funders Author Manuscripts